JOURNAL OF PROPULSION AND POWER
Vol. 26, No. 5, September–October 2010

Exploring the Effects of Nanostructured Particles on Liquid Nitromethane Combustion

Justin L. Sabourin,* Richard A. Yetter,† and Venkata Sharat Parimi‡
Pennsylvania State University, University Park, Pennsylvania 16802

DOI: 10.2514/1.48579

Monopropellants consisting of liquid nitromethane and high-surface-area particles of silicon- and aluminum-based oxides were examined to determine the effects of low concentrations of nanostructured materials on deflagration processes. The combustion rates were characterized by measuring linear burning rates in a large pressure vessel filled with argon. Results showed that nitromethane burning rates may be increased at lower pressures with dilute additions of particles. Increases in nitromethane burning rates of greater than 50% were found with less than 1.0 wt% of particle addition at a nominal pressure of 5.24 MPa. The particle additions were estimated to have only small effects on the equilibrium flame temperatures, density, viscosity, and specific heat. Nitromethane with particle additives displayed a lower burning-rate equation pressure exponent (i.e., reduced pressure sensitivity), which was inversely proportional to particle concentration. Above a pressure of approximately 9 MPa, up to the maximum test pressure (∼14 MPa), the particle additives did not affect the nitromethane burning rate. Condensed-phase temperature profiles of the deflagrating fluid, surface tension, and fluid thermal conductivities were measured in order to elucidate some of the mechanisms causing enhanced burning rates at lower pressures.

I. Introduction

THE last decade of research has created significant growth in the knowledge of the combustion dynamics involving nanostructured materials, particularly of metal nanoparticles, and their effects on larger-scale systems, such as explosives and solid propellant rockets. The exponential growth of this area, which continues today, has directly correlated with the development of materials science and manufacturing of nanostructured particles. These materials are being used as additives in liquid systems as well, producing promising results for future applications. Earlier studies involving liquid fuels with solid particles consisted mainly of slurry or gelled fuels, which contained high concentrations of additives [1]. More recently, researchers have found that nanostructured additives may be evenly dispersed within liquids for much longer periods of time than their micron-scale counterparts. Additionally, it has been demonstrated that even with small additions of nanostructured additives, combustion and heat transfer properties may be greatly influenced.

Enhancements in burning rates of both solid and liquid fuels have been obtained with large additions of metal nanoparticles [2–5]. These enhancements are attributed to the larger energy densities of the fuels with metal particle additives and to the short burning times of the particles, due to their small dimensions and high surface area to mass ratio. However, under very small concentrations of particle additives, energy densities are perturbed only slightly. Dilute concentrations of nanoscale additives, both energetic and nonenergetic, have demonstrated the ability to tailor combustion properties, indicating mechanisms are taking place beyond altering fuel energy densities [6–10]. Tyagi et al. [6] illustrated that ignition probabilities could be improved by dispersing aluminum or alumina nanoparticles (0–0.5% by volume) within diesel fuel. Hassan et al. [7] showed that multiwalled carbon nanotubes (MWCNTs) dispersed within 1-propanol can reduce flame spreading rates and increase ignition times at concentrations as low as 0.5 wt%. The presence of the MWCNTs was determined to enhance the heat transfer coefficient of the fuel. In a novel use of nanoparticles, alumoxanes have been used as a catalyst support and dispersed within hydrocarbon fuels, reducing ignition temperatures and increasing reaction rates [8]. It has also been proposed that dilute additions of CNTs or other nanoparticles may be used for the distributed ignition of fuels by light sources [10]. More recently, the dispersion of small concentrations of functionalized graphene sheets (FGSs) or solid oxide particles within the monopropellant nitromethane (NM) have exhibited significantly increased burning rates at lower pressures and therefore reduced burning-rate pressure dependence [9]. Burning rates enhancements of NM as large as 184 and 67% were found with 0.5 wt% FGSs and 0.96 wt% silica particle additives, respectively, at a nominal pressure of 5.24 MPa. Many of the mechanisms that lead to these significantly altered combustion dynamics are not understood; this paper addresses the effects of nanostructured oxide particle additives on both the chemical burning processes and physical properties of NM in order to decipher some of these mechanisms.

There are vast amounts of studies in the heat transfer field regarding nanofluids, which have shown many cases where small dispersions of nanoparticles within a liquid may greatly affect heat transfer properties. A nanofluid, a term coined by Choi [11], describes a dilute mixture of dispersed nanoscale particles within a liquid medium, which have been found to have some very intriguing properties to scientists and engineers. These nanofluid mixtures are more appropriately termed a colloid, or more specifically a sol, and the terms are used interchangeably throughout this text. Conductivity enhancements of greater than 20% are common with low particle concentrations [12], and a enhancement as large as 150% has been reported using engine oil with 1% (vol) CNTs dispersed within it [13]. A great deal of effort has been made to understand the mechanisms that create these large thermal transport enhancements. Das et al. [14,15] and Eastman et al. [16] have offered several good reviews of experimental and theoretical investigations involving the thermal transport of nanofluids in the last few years. This enhanced thermal energy transfer property is just one example of how dispersed nanoscale particles may affect thermal energy transfer of a liquid system. Since concentrations and diameters of particles in nanofluids are small, viscosity and density are generally not greatly affected. Nitromethane and other fuels are not considered heat

Received 22 December 2009; revision received 15 April 2010; accepted for publication 17 April 2010.

*Ph.D. Candidate, Department of Mechanical and Nuclear Engineering, 14 Research Building East. Student Member AIAA.
†Professor of Mechanical Engineering, 111 Research Building East. Member AIAA.
‡Ph.D. Candidate, Department of Mechanical and Nuclear Engineering, 14 Research Building East.

transfer fluids, except for in high-performance aircraft; therefore, no studies have been conducted that explore the effects of small concentrations of particles on NM thermal conductivity. In this report, the liquid thermal conductivity of NM was measured with and without particle dispersions.

Nitromethane was considered in this study and our previous study due to its ease of handling and its molecular simplicity. Most important, since it is a monopropellant, it behaves as a perfectly mixed fuel and oxidizer system (fuel-rich), removing many of complicated combustion dynamics associated with diffusion and mixing in bipropellant systems. Nitromethane is also highly energetic and may be used as a bipropellant component, or a high explosive. The nontoxic nature of NM, energy content, low viscosity, and ease of manufacture and handling make NM an interesting prospect for present and future propulsion and explosive technologies, as well as a good surrogate fuel for developing an understanding of the effects of dilute dispersions of nanoscale additives on liquid combustion. One unattractive feature of neat NM as a propellant is its high burning-rate pressure dependency. Understanding the chemical and physical processes that affect the pressure sensitivity of burning rates is still an important research topic. Because of its simple chemical structure, the fundamental knowledge gained from understanding how NM reacts to small amounts of nanostructured materials may help clarify that question, and also apply to other liquid mono- and bipropellants currently in use or under development.

Unlike metallic particles, oxide and hydroxide particles generally do not increase the energy content of a liquid monopropellant combustion system, but rather act as a small diluents [9]. Since these particles act as diluents, it is expected that using them as an additive should decrease burning rates; however, results indicate otherwise [5,9]. A previous study by Sabourin et al. [5] has indicated that enhanced linear burning rates of NM may be found with CAB-O-SIL® (i.e., silica) additions as high as approximately 4 wt%. Oxide particles are used in the current study because they are easily obtained and much easier to disperse in low-viscosity NM than metal particles for the required time intervals needed for experimentation, due to their porous structure and high surface areas. Additionally, since they have a negligible and/or negative effect on the energy content of NM, any enhancements in combustion processes may be attributed to the physical interaction and/or catalytic reactions between the oxide surfaces and NM, or the intermediate reaction species.

This investigation analyzes the effects of dilute dispersions of high-surface-area oxide particles within NM by examining the burning rates, as well as the thermal and physical properties of these mixtures. In addition, mechanisms are identified that affect these combustion processes. There are several other aspects of sols that may affect combustion of liquid fuels and monopropellants. Dispersions of small amounts of particles throughout a liquid provide heterogeneous nucleation sites for phase transformation, and may entrain themselves in the Stefan gas flow from the liquid surface. Entrainment of the particles into the gas phase may affect the radiation heat transfer coupling between the gas and liquid phase, particularly in optically transparent liquids. Because of the very large surface area of many nanoscale particles, they may act as in situ catalysts, or catalyst supports, for condensed and/or gas-phase reactions. The aim of the current research is to explore to what degree these issues affect the combustion rates of sols consisting of NM and various oxide particles.

II. Experimental Approach

The effects of the oxide particles on the combustion dynamics of nitromethane were characterized by measuring the linear burning rate within a fused quartz tube as a function of pressure and mixture composition. Nitromethane will not produce a self-propagating combustion process under atmospheric pressure in an argon environment and burns very slowly in air. Therefore, steady-state linear burning rates were obtained using an argon pressurized constant volume optical vessel (23 l) under well-controlled operating conditions. Real time recording of the combustion process was monitored using a digital video camera. The chamber, experimental setup, and basic procedure are described and shown schematically in previous publications [17,18].

Colloid samples were prepared in small batches within glass vials. Mixtures were measured on a mass basis using an analytical balance with a readability as low as 0.01 mg. The particles were dispersed manually within each vial before placing the samples into an ultrasonic bath for a minimum of 40 min to reduce particle agglomeration and limit air entrapment. All samples were sonicated immediately before testing, and then loaded into 10 mm quartz tubes (8 mm ID), which were a minimum of 6.5 cm long. Each quartz tube was capped at one end using hot craft glue. The quartz tubes allowed for the burning rates to be optically observed. Ignition of each sample was accomplished using an ignition booster made of double-base gun propellant (NOSOL 363), threaded over a strand of nichrome wire, which was placed slightly above the top of the liquid column. The nichrome wire was resistively heated by a power supply to ignite the booster, which in turn ignited the NM. A Nicolet Genesis multichannel data acquisition system monitored and recorded the system pressure as a function of time at a standard sampling rate of 500 Hz, while the receding liquid column was recorded using the digital video camera, allowing for linear burning rates to be determined (Fig. 1).

In addition to determining the effects of the additives on burning rates, we also explored the effects of particle addition on the condensed-phase temperature profile during the deflagration process. To accomplish this, the fused quartz tubes were fitted with a

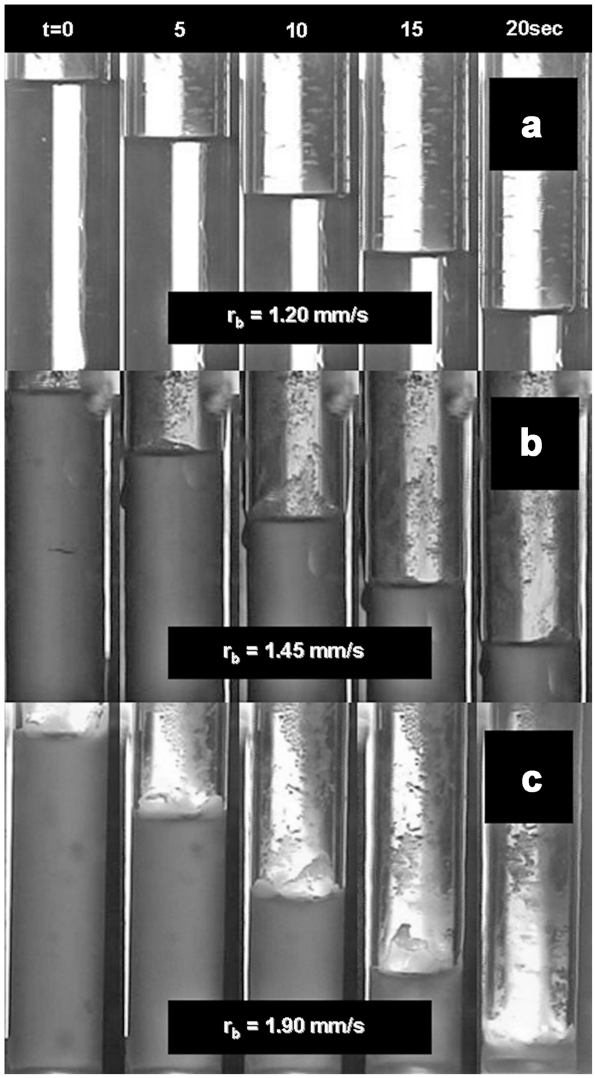

Fig. 1 Captured images of the combustion process of a) neat nitromethane, b) 0.057% Al_2O_3 plus/NM sol, and c) 0.37% porous spherical SiO_2/NM sol; (P_{ave} = 5.24 MPa).

single 25 μm E-type thermocouple (TC), which was procured from Omega Engineering, Inc. The TCs were placed into small diameter (1/32 in.) double bore alumina protection tubes with the junction protruding a minimum of 1 mm from the tip of the alumina tube. These assemblies were then mounted in the center of the quartz tubes so that the junction would contact the preheat zone and burning surface before all other components, ensuring the alumina tube would not affect temperature measurements (Fig. 2).

As part of this study, an effort was made to evaluate the thermal conductivity of the mixtures considered. This was important, due to the large amount of evidence suggesting that the thermal conductivities of sols (i.e., nanofluids) may be much greater than the neat fluid. The transient hot-wire (THW) method was used to measure the thermal conductivities of the nanofluids in consideration. The theory involved in the THW method is explained in detail elsewhere [19]. Advantages of the THW method are the elimination of natural convection under most conditions, and short measurement times. This method is often used for the measurement of liquid thermal conductivity and diffusivity, and has been used previously to measure these properties of nanofluids [20–22].

The THW method employs a thin wire suspended vertically in a liquid. The wire acts as both heat source and temperature sensor. The analytical model used for this method is derived for an infinitely long line source of heat in quiescent medium, which reduces to Eq. (1), where $T(t)$ is the temperature of the wire at time t, Q is the heat generated in the wire per unit length, k is the fluid thermal conductivity, α is the thermal diffusivity, r is the wire diameter, and γ is Euler's constant. In the time period when this solution is applicable ($t > \sim 0.2$ s), the increase in temperature is proportional to $\ell n(t)$, and the thermal conductivity of the liquid may be evaluated using Eq. (2):

$$T(t) - T_{\text{ref}} = \frac{Q}{4\pi k}\,\ell n\left(\frac{4\alpha t}{r^2\gamma}\right) \tag{1}$$

$$k = \frac{Q}{4\pi[T(t_2) - T(t_1)]}\,\ell n\left(\frac{t_2}{t_1}\right) \tag{2}$$

In the current work, a platinum (Pt) wire 51 μm in diameter was used. The temperature of the wire was determined by using its stable temperature-resistance relationship, which was correlated with high accuracy using a linear relationship. To avoid electrical interference, the wire and all parts of the apparatus in contact with the fluid were coated with a 2-μm-thick insulating layer of Parylene N (Specialty Coating Systems, Indianapolis, Indiana), a commercially available polymer material used in vapor deposition processes. Advantages of this thin polymer coating are that is it an excellent dielectric with good chemical- and moisture-barrier properties. The length of the Pt wire was 75 mm and the inner diameter of the test cell, which was a fused quartz test tube, was 18 mm. A schematic of the test setup is shown in Fig. 3. The test chamber was placed in a temperature-controlled circulating-water bath to maintain a constant temperature. The Pt wire served as one of the resistive arms of a Wheatstone bridge. As current was passed through the Pt wire it resistively heated, also causing the resistance to change. The output voltage of the bridge was amplified and recorded using a National Instruments data acquisition card (NI PCI-6036E) with a sampling frequency of 100 Hz. This voltage was then used to calculate the heating rate of the wire, which was a function of the thermal conductivity of the fluid surrounding the wire. Calibration of the system was performed using toluene and methanol as standard fluids. The calibration was then validated using water and isopropyl alcohol, two liquids with well-known and widely different thermal conductivities. Each individual testing period lasted the order of 1 s to capture enough data for evaluation of the fluid thermal conductivity.

Sols were prepared using the same method as in the combustion tests; however, an ultrasonifier (Branson Digital Sonifier S-450) was used instead of the bath sonicator. The nanofluids were sonified a minimum of 5 min using the ultrasonifier to break up agglomerates and evenly disperse the particles before any testing and then repeatedly between each measurement for an additional 2 min. Once the test cell was placed in the water bath, the fluid was quickly brought to the desired test temperature and allowed to equilibrate for 1–2 min, removing any remaining convective currents.

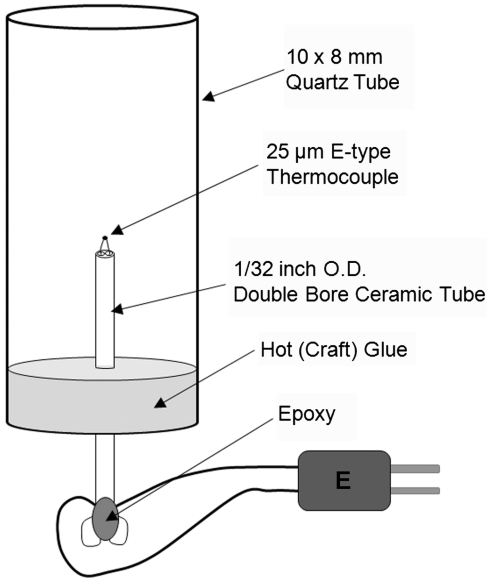

Fig. 2 Schematic of the setup used for measuring condensed-phase temperature profiles of the deflagrating monopropellant.

III. Material Properties and Characterization

Nitromethane, used as the fuel sol dispersion medium, is a polar, transparent, and low-viscosity liquid at standard atmospheric conditions. Because of its use in chemical processes as well as propulsion, many of the important thermodynamic, fluid dynamic, and heat transfer properties of both liquid- and gas-phase NM have been characterized [23–26]. Of particular interest to this investigation is the saturation pressure, correlated as a function of saturation temperature, which may be estimated as the liquid surface temperature of deflagrating NM [Eq. (3) [25]]. Equation (3) is valid up to the critical conditions ($P_{\text{crit}} = 6.3126$ MPa and $T_{\text{crit}} = 588.15$ K), and the temperature and pressure are expressed in units of Kelvin (K) and Pascal (Pa). Nitromethane used in this study was procured from Sigma-Aldrich and was greater than 98% chemically pure [Chemical Abstracts Service (CAS) no. 75-52-5)].

$$P_{\text{sat}} = \exp\left[87.41 - \frac{7133}{T_{\text{sat}}} - 9.779\,\ell n(T_{\text{sat}}) + 7.906 \times 10^{-6} \cdot T_{\text{sat}}^2\right] \tag{3}$$

Four different solid oxide materials were used in this study: two silica-based and two amorphous-alumina-based. These particles

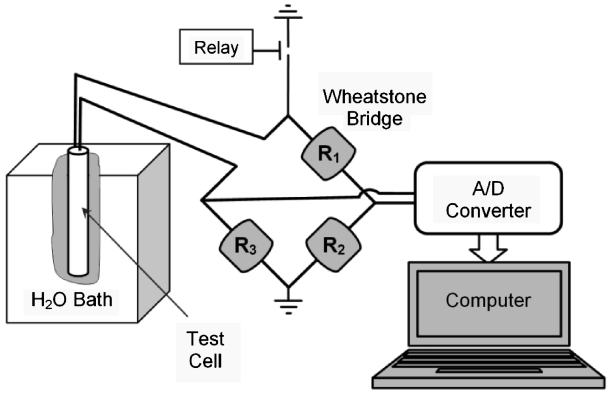

Fig. 3 Schematic of the THW method used for liquid thermal-conductivity evaluation.

were chosen due to their porous structure, creating high specific surface areas (SSAs, m^2/g), maximizing possible nucleation or catalyst area per unit mass addition, and increasing dispersion times. Previous studies of nanofluids have also shown a correlation between SSA and base-fluid thermal-conductivity enhancement, as represented by increased SSA with decreased particle diameter [14]. Both silica particles were procured from Sigma-Aldrich, while the alumina particles were purchased from NanoScale Corporation (Manhattan, Kansas). The amorphous alumina particles (as described by the supplier) have been demonstrated to be more appropriately labeled aluminum monohydroxide (AlOOH) in previous work [9]. Table 1 presents physical properties of each particle that are either provided by the supplier or determined experimentally as part of this study. All volumetric values provided throughout this study are calculated using density values determined using a helium pycnometer.

Scanning electron microscopy images are shown in Fig. 4. Alumina-based particles (NanoActive Al_2O_3 and Al_2O_3 plus, Figs. 4a and 4b, respectively) obtained from NanoScale Corporation were larger in overall dimensions than the silica particles. The first silica particle (Fig. 4c) was spherical and porous, with very small diameter and high surface area (CAS no. 7631-86-9), while the second silica particle (Fig. 4d) was mesostructured with a hexagonal framework (MCM-41) and also had a very high surface area (CAS no. 112945-52-5). Although several of the particles considered did not have nanometer overall dimensions, all particles were dominated by nanoscale features, due to their porous structure. These nanoscale pores had diameters on the scale of 11 nm or less, which were beyond the resolution of the scanning electron microscopy (SEM) images shown. Since the large SSA of nanoparticles leads to many of their unique features pertaining to thermal energy transport and reactivity, these large particles were assumed to demonstrate many of the unique properties of nanoparticles, and in this study the term nanofluid was extended to include particles dominated by nanoscale pores, creating extremely large specific surface areas.

The properties of the sols, which contained a maximum of 1.7 wt% oxide particles, were assumed to be altered very little from that of neat NM. Indeed, surface-tension measurements indicated a slight but negligible reduction ($\sim$1.5%) with the sols verses the neat liquid cases (Table 2), which was in agreement with previous investigations of surface tension [14,27]. Based on rheological studies of nanofluid viscosity, a maximum increase of 7.5% was expected at the highest particle concentrations studied using simple theory; however, most experiments indicated increases that were considerably less [28,29]. An Einstein model predicted viscosity increases of less than 2% (Table 2). The sol densities were not calculated using an experimental method but rather evaluated using Eq. (4), where φ is the volume fraction of particles, and the subscript f and p stand for fluid and particle, respectively. Volumetric fraction of particles was calculated using Eq. (5), where x is the mass fraction determined during mixing:

$$\rho = (1-\varphi)\rho_f + \varphi\rho_p \tag{4}$$

$$\varphi = \frac{x\rho_f}{(1-x)\rho_p + x\rho_f} \tag{5}$$

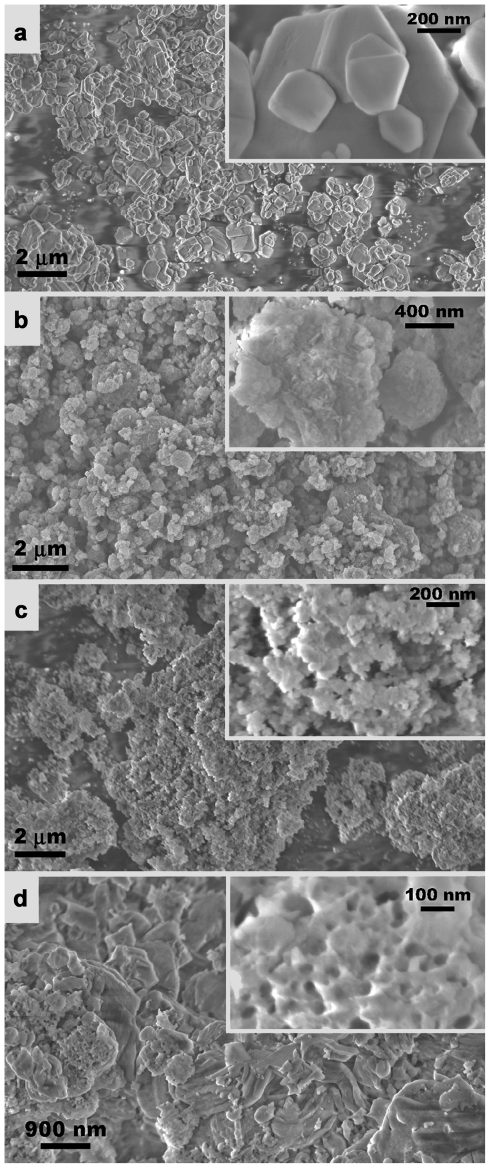

Fig. 4 SEM images of particles: a) NanoScale Corporation Al_2O_3, b) NanoScale Corporation Al_2O_3 plus, c) SiO_2 (spherical porous), and d) mesoporous SiO_2 (MCM-41).

Simple calculations indicated that sol density was increased, while specific heat was decreased with particle addition; however, both changed minimally.

The results of the thermal-conductivity evaluation are shown in Table 3. These results indicated that the THW method produced good results and that the Parylene coating did not affect results, as the measured thermal conductivities of the standardized fluids (i.e., deionized water and isopropyl alcohol) were calculated with

Table 1 Physical characterization of particles[a]

Particle	ρ, g/cm^3	ρ_{bulk}, g/cm^3	Surface area[b], m^2/g	Pore volume[c], cm^3/g	Avg pore diameter[c], nm
Mesoporous silica (MCM-41)	2.08	0.34[d]	1070 ($\sim$1000)[d]	1.087 (0.98)[d]	3.3 (2.7)[d]
Silica, 5–15 nm[d] (spherical, porous)	2.0 (2.2–2.6)[d]	0.068[d]	570 (590–690)[d]	0.42	5.3
NanoActive aluminum oxide	3.05 (3.9)[d]	0.5[d]	330 (>275)[d]	0.27 (>0.15)[d]	3.2 (2.8)[d]
NanoActive aluminum oxide plus	2.7 (2.9)[d]	0.20[d]	530 (>550)[d]	1.33 (>1.50)[d]	8.2 (11.0)[d]

[a]Density measurement was made using Micromeritics AccuPyc 1340, and surface-area and porosity measurements were made using Micromeritics ASAP 2020.
[b]From BET (Brunauer, Emmett, and Teller) adsorption theory.
[c]From BJH (Barrett, Joyner, and Halenda) adsorption theory.
[d]Manufacturer- or supplier-given value.

Table 2 Nitromethane sol properties and characterization ($T = 19.8°C$)

Fluid or sol, % mass (% vol.)	Density, g/cm^3	Surface tension [a], dyne/cm $\pm 2\sigma$	Viscosity, mPa-s	Specific heat, J/mol-K
100 (100)% NM	1.137 [25]	36.98 $\pm$ 0.13, 37.01 [24]	0.672 [24]	106.2 [25]
0.44 (0.28)% SiO_2/NM	1.139 [b]	36.53 $\pm$ 0.13	0.677 [b]	105.9 [b]
0.87 (0.55)% SiO_2/NM	1.141 [b]	36.50 $\pm$ 0.08	0.681 [b]	105.6 [b]
1.26 (0.57)% Al_2O_3 plus/NM	1.145 [b]	36.61 $\pm$ 0.18	0.682 [b]	105.3 [b]

[a]Using a SensaDyne PC9000 bubble tensiometer.
[b]Calculated using Eqs. (4), (5) or (6) of [16].

Table 3 Thermal conductivity of fluids and sols

Fluid	Temp, °C	Reported k, W/m-K	Model prediction from [30], W/m-K [a]	Measured k, W/m-K: Average	σ	% Deviation from the reported k of the neat fluid
Isopropyl alcohol	25	0.135 [26]	——	0.132	0.0004	−2.2
Deionized H_2O	25	0.608 [26]	——	0.610	0.005	+0.33
100% NM	25	0.207 [24]	——	0.208	0.003	+0.48
1% (wt.) SiO_2/NM	25	——	0.210 (+1.3%)	0.202	0.001	−2.4
100% NM	15	0.211 [24]		0.202	0.001	−4.3
1% (wt.) SiO_2/NM	15	——	0.214 (+1.2%)	0.211	0.003	+0.0
Deionized H_2O	35	0.622 [26]	——	0.636	0.005	+2.3
1% (vol.) CuO/H_2O	35	——	0.640 (+2.9%)	0.708	0.014	+13.8

[a]Predicted heterogeneous two-phase thermal conductivity based on conventional model developed by Hamilton and Crosser [30].

satisfactory levels of error, as was neat NM. From the burning-rate results, nanoscale porous SiO_2 particles provided the greatest burning-rate enhancement of NM, and were observed to have the greatest dispersion stability. For this reason, it was believed that this mixture may display the greatest increase in thermal conductivity. However, the results indicated that the conductivity was slightly decreased at 25°C. At 15°C there appeared to be an increase in the measured sol conductivity over neat NM; however, there was no difference between the sol and previously reported value. Unfortunately, higher-temperature data could not be gathered when using NM, due to the onset of natural convection affecting the results. For further verification of the THW system, comparisons were made to previous nanofluid heat transfer studies. A mixture of CuO (Sigma-Aldrich, CAS no. 1317-38-0, 33 nm, 27 m^2/g) and deionized H_2O was studied for this purpose. This mixture displayed a significant increase in thermal conductivity with 1% particle addition (13.8%). A very similar mixture was studied by Das et al. [31], who analyzed a nanofluid mixture containing 28.6 nm nominal diameter CuO particles. Their study used a different experimental technique and found an enhancement of ~20% at 35°C and 1% particle loading. From the data gathered it was concluded that the silica and aluminum hydroxide particle additions did not affect the thermal conductivity of NM at room temperatures; however, it is still unknown how higher temperature and pressure conditions may alter heat transfer properties.

IV. Results of Deflagration Analysis

The linear burning rates of sol colloids composed of nitromethane and various solid oxides were determined as a function of pressure (3.25–13.9 MPa) and mixture composition (0–1.69 wt%, 0–0.61%). From Fig. 1 it is shown that the sols were much less transparent, due to the light scattering and absorption properties of the particles. No visible flame was seen with neat NM except for at higher pressures. A visible flame appeared with the sols, due to entrained particles radiating at high temperature. The liquid surface was altered slightly with particle addition as well. In the neat-NM case, the surface was very flat and little to no bubbling or waves were seen. However, the sols showed some waves at the surface, and some increased bubbling near the surface, though neither was consistently observed. It was unclear if the wavy surface was consistent throughout the cross section of the tube, or if it was a wall effect. The images also show coating of the tube walls and some layering of particles at the surface at lower pressures. The extent to which the surface was altered increased with particle concentration.

Figure 5 illustrates the constant pressure burning rate of the four different sols considered as a function of particle addition. In all cases the linear burning rate increased with increasing particle addition. Compared to neat NM, burning rates were enhanced by greater than 55% in three of the four sols with only 1 wt% particle addition. All of these particles had a SSA greater than 500 m^2/g; the lowest degree of enhancement was found with the smallest SSA (largest overall dimension) particles (i.e., Al_2O_3). As a caveat, these larger particles also produced the least stable suspension. Therefore, it is not clear at this time what role colloid stability plays in producing the burning-rate enhancements, future work in this area should address this issue. Figure 6 shows the same plot as a function of volume concentration.

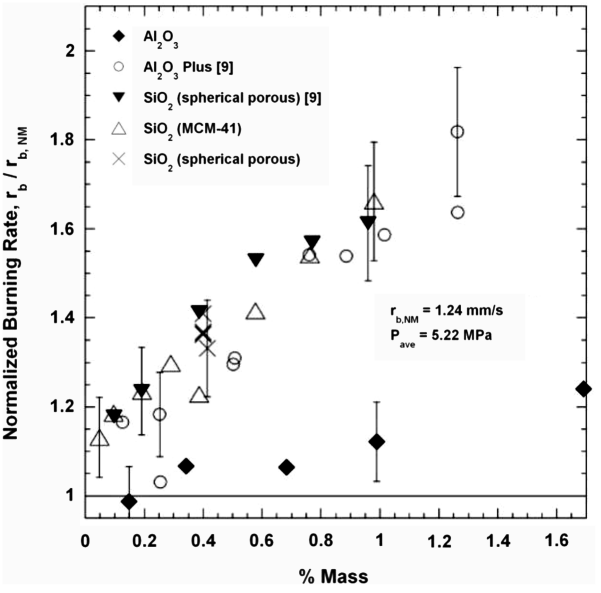

Fig. 5 Burning-rate enhancement as function of particle addition (% mass).

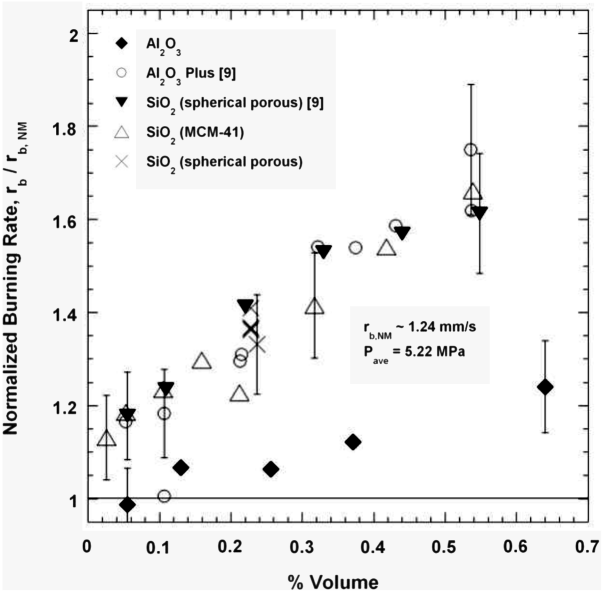

Fig. 6 Burning-rate enhancement as a function of particle addition (% volume).

An interesting aspect of these results are that the MCM-41 particles, which had by far the greatest SSA, enhanced the burning rates approximately the same amounts as Al_2O_3 Plus and spherical porous SiO_2 nanoparticles. These particles have very small pore sizes as well (Table 1), which may indicate that pore sizes below a certain value are less effective at enhancing the interaction between NM and the particles. It should also be noted that the lower SSA Al_2O_3 particles had pores sizes nearly identical to that of the MCM-41. Overall, these results indicated that oxide type plays little role in the enhanced burning process, and the surface area and morphology play a much stronger role; however, there may be an upper limit at which increases in SSA no longer affect burning rates.

Figure 7 displays the linear burning-rate pressure dependence of two sols (0.76 wt% Al_2O_3 Plus and 0.58 wt% porous SiO_2), as well as the baseline NM case. Results show that under the range of pressures considered, the sols were less sensitive to pressure than the neat NM. This indicates that the effects of the particles were diminished at higher pressures, and the homogeneous combustion process of the neat NM dominated. Since it was not possible with the current setup to go to higher pressures, it is unclear if the sols would maintain the lower pressure dependence at pressures greater than 14 MPa, or if the sols would follow the same pressure dependence of the neat NM, although our interpretation of the enhancement mechanisms suggests the latter. Over the range of pressures considered, sols exhibited burning-rate pressure exponents of 0.81 and 0.80 for Al_2O_3 Plus and spherical porous SiO_2 particles, respectively. This was a reduction of approximately 0.4 from neat NM ($n = 1.2$). Burning rates of neat NM are verified by Boyer and Kuo, who determined a pressure exponent of 1.17, using a quartz tube sample holder [32]. It should be noted that this previous study also described three burning-rate pressure regimes for NM. At pressures between 15 and 70 MPa, the pressure exponent increased to 2.33, before reducing to 0.86 in the highest pressure range.

Figure 8 emphasizes the greater influence of particle dispersions at lower pressures. In this figure, linear burning rates are plotted as a function of spherical porous SiO_2 nanoparticle concentration at two different pressures. The plot clearly indicates a much greater dependence on concentration at the lower pressures. Burning rates of NM were enhanced by approximately 53% (0.68 mm/s) at an average pressure of 5.3 MPa, versus only 6.4% (0.15 mm/s) at 8.96 MPa with 0.77 wt% porous SiO_2. These results suggested that burning-rate pressure exponents may be decreased to values below 0.8 at concentrations greater than those presented in Fig. 7. Conversely, pressure exponents should increase towards that of neat NM at lower concentrations of inert particles.

The measured temperature profiles of two different mixtures, neat nitromethane and a 0.4 wt% porous silica sol are shown in Fig. 9. Using Eq. (3), the surface temperature of the burning NM was estimated to be 300°C, which is very close to the point of inflection of the neat-NM tests. The inflection point is generally regarded as the surface temperature of a condensed-phase propellant. It should be noted that all curves in Fig. 9 were arbitrarily set so that the estimated surface temperature was at zero in the plot. Using technical data provided by Omega regarding the response time of 25 μm diameter TCs (i.e., 0.002 s in still H_2O), and the measured burning rates of the mixtures presented, a resolution equal to the TC junction diameter was expected (i.e., ~0.05 mm). The results of the sols condensed-phase burning profile were not reproducible. Variations were assumed to be from flexing of the TC wires, TC junction interaction with oxide particles, and other experimental irregularities. One of these irregularities was identified using the video of the burning process. Many of the particles were caked onto the sides of the tube following the combustion wave, which sometimes fell from the wall into the burning mixture, creating subsurface bubbling in the liquid.

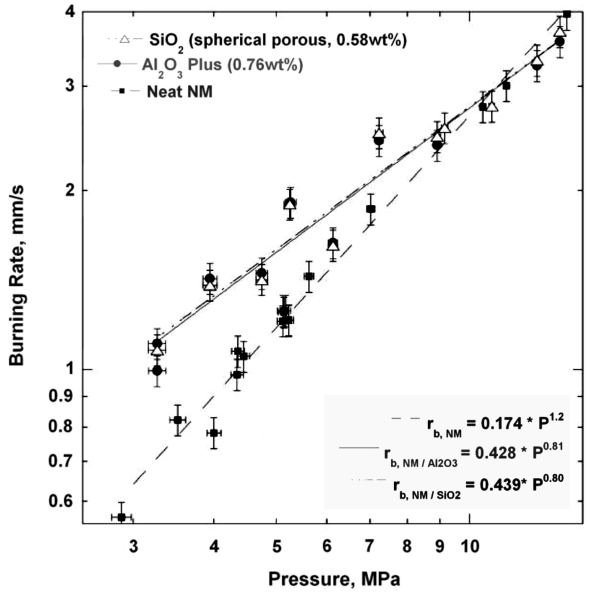

Fig. 7 Burning rates as a function of pressure.

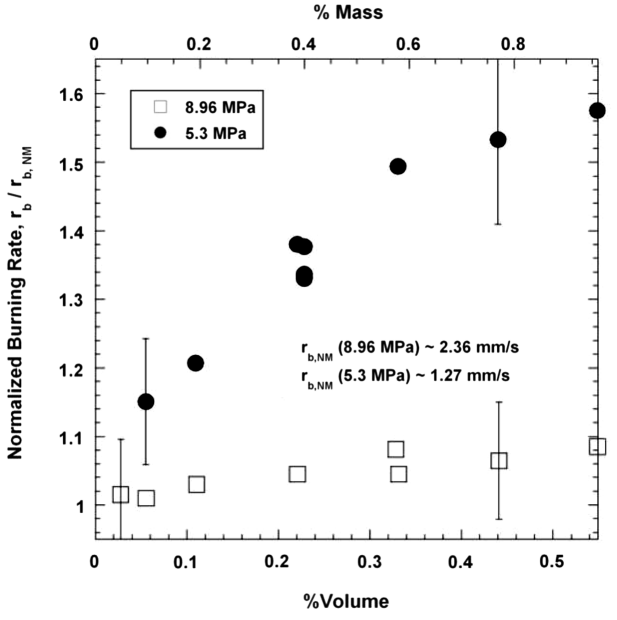

Fig. 8 Burning rates as a function of porous silica nanoparticle addition at average pressures of 5.3 and 8.96 MPa.

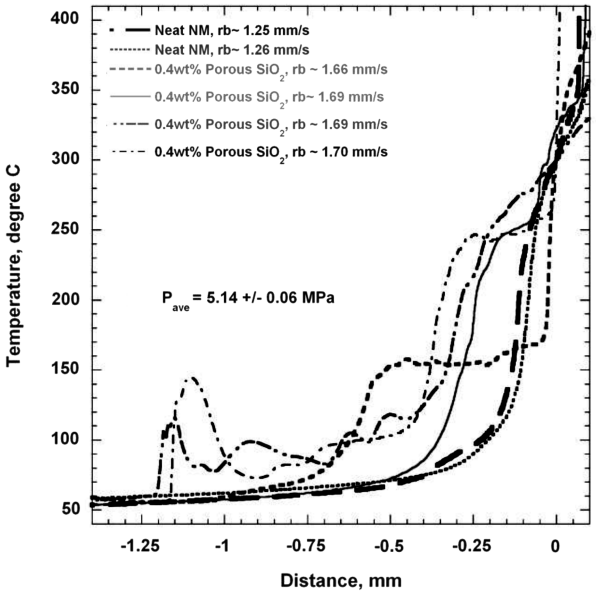

Fig. 9 Temperature profiles of burning processes.

This process corresponded to large jumps in the condensed-phase profile of two experimental runs, shown between −1.0 to −1.25 mm in the figure. It is important to observe that these jumps in temperature were quickly equilibrated. The effects of these occurrences on the overall burning rate were determined to be negligible by varying the diameter of the quartz tube (Fig. 10). Internal quartz tube diameters of 12 and 22 mm were used in addition to the standard 8 mm tube. All tube diameters produced the same burning rates with both neat NM and sols of 0.4 wt% porous SiO_2. There were few conclusions that could be drawn from Fig. 9, due to these peculiarities; however, they did indicate that the thickness of the condensed-phase heated region was increased with particle addition, even though the mixtures were burning at a faster rate. Initially, this indicated that the thermal conductivities (or diffusivity) of the mixtures were appreciably greater than that of neat NM. However, we measured the thermal conductivity of a 1 wt% mixture to have no difference from that of neat NM. This implied that another heat transfer mechanism was taking place, most notably radiation, or there was a remarkable increase in the sol's thermal diffusivity at higher temperatures that was not present at room temperature. There is evidence of a strong temperature dependence occurring with nanofluid systems; however, in all of these cases there was an enhancement at room temperature as well [31].

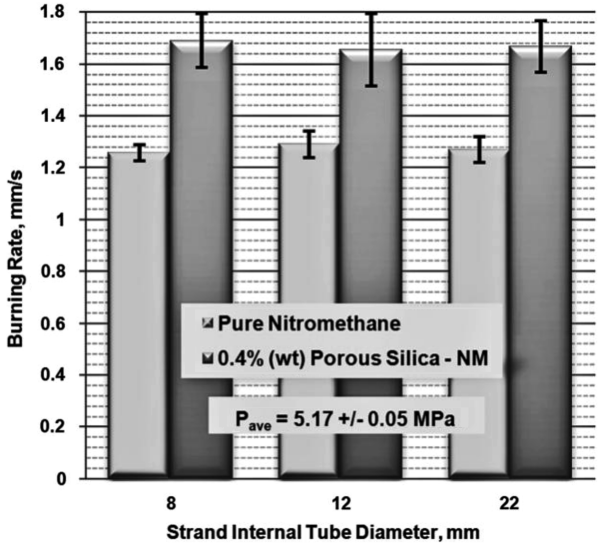

Fig. 10 Effect of strand internal diameters on burning rates.

V. Discussion

The results show that NM burning rates were increased with increasing particle addition, but the relative enhancement was reduced with increasing pressure as homogeneous NM reactions dominate heat release and transfer mechanisms. For the particles studied here, the enhancement was indicated to be a greater function of particle surface area than the material composition. Dispersion stability, which appeared to play a role in the burning-rate enhancement, was aided by high-surface-area particles as well. In fact, dispersion of 15 nm nominal diameter silica particles (Sigma-Aldrich, CAS no. 7631-86-9, SSA of 140–180 m^2/g) were attempted to be used without success. Mindful of these primary conclusions, a simple theoretical analysis was applied in order to identify physical and chemical mechanisms creating the burning-rate enhancement. Assuming a steady-state, one-dimensional burning process, with negligible heat losses through the tube walls (verified by using various tube diameters), a conservation of energy analysis was applied at the surface of the burning NM. The system is described schematically in Fig. 11. Given these conditions, with the assumption that the particles did not create a two-phase NM reaction zone, Eq. (6) may be used to describe the burning process, where the subscript p and r refer to preheat and primary reaction zones, respectively. The only variables or terms that are believed to vary with particle addition are the reaction-zone thickness δ_r, radiation heat transfer $q_{\text{radiation}}$, reaction-zone thermal conductivity k_r, or the area terms. Since the vaporization of NM occurred at a free surface, it is unlikely that the surface temperature was affected by particle additions:

$$r_b = \frac{[k_r A_r (T_R - T_{\text{surface}})/\delta_r] + q_{\text{radiation}}}{\rho_{\text{nanofluid}} A_{\text{tube}} [C_{p,\text{ave}} (T_{\text{surface}} - T_{\text{initial}}) + \Delta H_{\text{vaporization}}]} = \frac{\dot{m}}{\rho_{\text{nanofluid}} A_{\text{tube}}} \tag{6}$$

Using this equation, several mechanisms were identified that may enhance the burning rates of sols or nanofluids compared to neat NM. Using basic premixed flame theory, all mechanisms increase burning rates by increasing heat transfer from the exothermic chemical reactions back to the condensed phase, thereby increasing the efficiency of the chemical reactions' ability to propagate a flame. Condensed-phase reactions were assumed not to occur, even if small gas-phase bubbles were formed. This assumption has been verified to be accurate by Boyer and Kuo [33] for the neat-NM system. Given that the energy density of the nanofluid system was not increased with particle addition, the enhanced burning rate could only occur due to increased levels of heat transfer from the reaction zone, due to improved reaction-zone thermal conductivity k_r, radiation feedback from the gas-phase reactions back to the condensed phase ($q_{\text{radiation}}$),

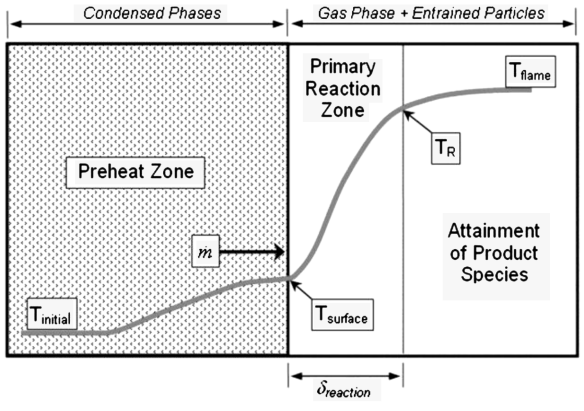

Fig. 11 Diagram of burning process and phase interface.

and/or a thinned primary reaction zone δ_r. The theory presented here indicates that steady-state burning rates were independent of condensed-phase thermal diffusivity. This was confirmed with simplified modeling of droplet evaporation/vaporization as well [34]. An additional physical mechanism was created by induced surface instabilities or roughness due to wetting of the high-surface-area particles at the liquid–gas interface, creating multiple surface interactions that increased liquid vaporization rate by increasing the free surface area. All of these mechanisms operated simultaneously, particularly at low pressures. As a result it was difficult to reconcile experimentally if a dominant mechanism existed. Each mechanism is discussed in more detail in the following paragraphs.

The increased radiation feedback occurred due to presence of the particles in both the liquid and gas phases. Entrained particles, or particles lying at the phase interface, emitted and absorbed radiation, as did the particles in the condensed phase, coupling radiation heat transfer between the two zones. Solids are known to absorb/emit a wide spectrum of thermal radiation [35], and nanoscale particles are known to have significantly altered optical properties compared to large-scale bulk materials [36]. Evidence that radiation heating was occurring may be found by closer examination of Fig. 9. In the tests shown in this figure, the burning rates were increased by ~34% with 0.4 wt% porous SiO_2, even though the condensed-phase heating process occurred over a wider length. Reviewing previous literature regarding thermal-conductivity enhancements [12], this burning-rate enhancement exceeded the estimated effect due to conductivity enhancements found in most other studies, although none of these studies approached the temperatures found in the near-surface region of the burning fluid. This information, along with our results indicating no fluid thermal-conductivity enhancement at room temperature, implied that radiation was playing a role in increasing the NM burning rate. Enhanced radiation heat transfer may also be assumed to be fairly independent of system pressure, since the NM flame temperature is not a strong function of pressure [25], which agrees with the burning-rate pressure dependence found here. As pressure increases the flame zone thickness decreases, increasing the temperature gradient, the driving force for heat conduction back to the surface. At the highest pressures considered, the dominant mechanism would be conductive heat transfer from the homogeneous gas-phase reactions back to the vaporizing surface. The results did not indicate that the chemical composition of the particles played a significant role. The fact that the emissive properties of alumina and silica are not equivalent and that the burning-rate enhancements were so large indicated other mechanisms were occurring in addition to enhanced radiation.

Catalytic processes, which were likely the most dominate mechanism, reduced reaction-zone thicknesses and increased burning rates in the manner found in our results. The particles, which had high melting points, may have acted as catalysts for the decomposition of NM or reduced the time scales associated with the dark zone chemistry of NM combustion [9,37]. However, there is limited data involving the catalytic properties of aluminum hydroxides and silica on NM. Yamaguchi [38] has indicated that NM chemisorbs onto γ-alumina, forming aci-anions ($CH_2NO_2^-$), a compound that has been identified as a sensitizing and rate-controlling species in the detonation of liquid NM [39]. The homogeneous decomposition of nitromethane ($CH_3NO_2 \rightarrow CH_3 + NO_2$) is a very endothermic process; therefore, opening an alternative chemical decomposition route (such as O removal from the nitro group [40]) could greatly improve ignition delays and reduce flame thickness [9]. From the video images it was clear that some particles were entrained in the gas flow, and a thin layer of particles did form at the surface of the burning mixture, both of which could have served as heterogeneous catalysts.

The presence of these particles increased energy feedback upstream of the primary reaction zone through conduction and radiation heat transfer. The particles also increased the heat capacity of the near-surface region of the primary reaction zone. This mechanism combined with catalysis drew the flame closer the surface (i.e., reduced δ_r) and increased vaporization rates of liquid NM. As with radiation, decreasing flame thickness with increased pressure (increased gas-phase collisions) may reduce the effects of these mechanisms on the burning rate to negligible levels. Catalysis is a heterogeneous process and therefore less pressure-sensitive than homogeneous gas-phase processes. Additionally, as burning rate increased, the formation of a particle layer at the surface was restricted, since most of the particles are entrained into the developed gas flow. Therefore, the homogeneous NM combustion reactions dominated at high pressures.

The final mechanism, a physical interaction between the high-surface-area particles and the NM, caused the interface area (i.e., A_r) between the gas and liquid phases to increase, increasing vaporization rates. Being a slightly viscous solvent, nitromethane therefore wets solid surfaces very well. When a layer of particles formed at the surface, the particles were wetted by the liquid NM, increasing the vaporizing area; the burning rate is equivalent to the vaporization rate, which is proportional to the surface area. This effect explained one of the reasons why the specific surface area of the particles played a significant role in the burning-rate enhancement. However, as critical pressures and temperatures are exceeded, this interaction between the liquid NM and particles was lost, and therefore did not play a role at moderate to high pressures.

Similar burning-rate pressure dependency effects as found here have been observed in studies involving solid propellant mixtures with small additions (1 wt%) of chopped Kevlar fibers [41]. Brewster et al. [41] found that addition of these fibers increased burning rates of both aluminized and nonaluminized ammonium perchlorate and hydroxyl-terminated polybutadiene propellants at low pressures (less than 5–8 MPa). The enhancement was greater in the aluminized propellant. As with this study, it was determined that dispersion of the fiber additive played a key role in the enhancement. The authors stated that the Kevlar fibers, which were flame-retardant, protruded from the burning surface during combustion acting as a flameholder, bringing the flame front closer to the surface than would normally occur at lower pressures. Unfortunately, this conclusion was not elaborated upon and no physical explanation was provided; however, the role of the fibers was similar to the role of the oxide particles. Both the fibers and the particles roughened the phase interface and protruded into the gas-phase reaction zone, which increased heat transfer rates, leading to enhanced vaporization and/or pyrolysis rates.

VI. Conclusions

Analysis of the burning rates of nanofluids or fuel sols consisting of nitromethane and various solid oxide particles has shown that liquid monopropellant burning rates may be enhanced at low pressures by dispersing ultrafine particles within the liquid. Burning rates are enhanced with increasing particle concentration at pressures below approximately 9 MPa. The rate enhancements of sols are greater as pressure is reduced; however, rates between 9 MPa and the maximum test pressure, 13.9 MPa, are within experimental error of neat NM. The burning-rate pressure exponents of sols are therefore reduced with increasing particle concentration, falling below unity at pressures below 9 MPa. Since the particles are chemically stable they act as slight diluents during NM burning, even though they increase burning rates at low concentrations. This result is encouraging as sols may reduce pressure sensitivity of liquid fuels or propellants, while increasing performance without significant loss of overall energy density.

Several mechanisms are identified that contribute simultaneously to increase the burning rate. These mechanisms include enhanced radiation and conduction heat transfer, increased reaction rates due to heterogeneous catalysis, and an increased phase interface area, all of which increase upstream energy transport into the condensed-phase NM, which in turn increases burning rates. At high pressure these mechanisms are overcome by homogeneous gas-phase processes involving NM combustion, since the enhancement mechanisms are less pressure-sensitive. Material characterization conducted here and review of previous literature has shown than sols do not significantly affect fluid dynamic or heat conduction properties of the neat NM.

Acknowledgments

This work was sponsored by the U.S. Army Research Office under the Multi-University Research Initiative, contract no. W911NF-04-1-0178. The support and encouragement provided by Ralph A. Anthenien is gratefully acknowledged. Additionally, the authors would like to thank the help and support of Magda Salama of the Materials Characterization Laboratory at Pennsylvania State University (PSU) for her help with particle testing and analysis, and BaoQi Zhang of the PSU's High Pressure Combustion Laboratory for his help making the thermocouples used for condensed-phase temperature measurements.

References

[1] Natan, B., and Rahimi, S., "The Status of Gel Propellants in Year 2000," *Combustion of Energetic Materials*, edited by K. K. Kuo, and L. deLuca, Begell House, Boca Raton, FL, 2001, pp. 172–194.

[2] Kuo, K. K., Risha, G. A., Evans, B., and Boyer, E., "Potential Usage of Energetic Nano-Sized Powders for Combustion and Rocket Propulsion," *MRS Proceedings*, Boston, Vol. 800, 2004, pp. 3–14.

[3] Mench, M. M., Yeh, C. L., and Kuo, K. K., "Propellant Burning Rate Enhancement and Thermal Behavior of Ultra-Fine Aluminum Powders (Alex)," *29th International Annual Conference of ICT*, Karlsruhe, Germany, Vol. 30, 1998, pp. 1–15.

[4] Weiser, V., Eisenreich, N., Kelzenberg, S., Plitzko, Y., and Roth, E., "Influence of ALEX and Other Aluminum Particles on Burning Behavior of Gelled Nitromethane Propellants," *International Autumn Seminar on Propellants, Explosives and Pyrotechnics (2005IASPEP)*, Beijing, 2005, pp. 838–846.

[5] Sabourin, J. L., Yetter, R. A., Asay, B. W., Lloyd, J. M., Sanders, V. E., Risha, G. A., and Son, S. F., "Effect of Nano-Aluminum and Fumed Silica Particles on the Deflagration and Detonation of Nitromethane," *Propellants, Explosives, Pyrotechnics*, Vol. 34, No. 5, 2009, pp. 385–393.
doi:10.1002/prep.200800106

[6] Tyagi, H., Phelan, P. E., Prasher, R., Peck, R., Lee, T., Pacheco, J. R., and Arentzen, P., "Increased Hot-Plate Ignition Probability for Nanoparticle-Laden Diesel Fuel," *Nano Letters*, Vol. 8, No. 5, 2008, pp. 1410–1416.
doi:10.1021/nl080277d

[7] Hassan, M. I., Grulke, E., Chuah, K., and Saito, K., "Effects of Carbon Nanotubes on Flame Spread Rate over 1-Propanol," *Fire safety Journal*, Vol. 40, No. 5, 2005, pp. 425–438.
doi:10.1016/j.firesaf.2005.02.007

[8] Wickham, D. T., Cook, R. L., De Voss, S., Engel, J. R., and Nabity, J., "Soluble Nano-Catalysts for High Performance Fuels," *Journal of Russian Laser Research*, Vol. 27, No. 6, 2006, pp. 552–561.
doi:10.1007/s10946-006-0034-8

[9] Sabourin, J. L., Dabbs, D. M., Yetter, R. A., Dryer, F. L., and Aksay, I. A., "Functionalized Graphene Sheet Colloids for Enhanced Fuel Combustion," *ACS Nano*, Vol. 3, No. 12, 2009, pp. 3945–3954.
doi:10.1021/nn901006w

[10] Chehroudi, B., Vaghjiani, G. L., and Ketsdever, A. D., "Method for Distributed Ignition of Fuels by Light Sources," U.S. Patent 7,517,215 B1, 14 April 2009.

[11] Choi, S. U. S., "Enhancing Thermal Conductivity of Fluids with Nanoparticles," *ASME International Mechanical Engineering Congress and Exposition*, American Society of Mechanical Engineers, New York, 1995, pp. 99–105.

[12] Yu, W., France, D. M., Routbort, J. L., and Choi, S. U. S., "Review and Comparison of Nanofluid Thermal Conductivity and Heat Transfer Enhancements," *Heat Transfer Engineering*, Vol. 29, No. 5, 2008, pp. 432–460.
doi:10.1080/01457630701850851

[13] Choi, S. U. S., Zhang, Z. G., Yu, W., Lockwood, F. E., and Grulke, E. A., "Anomalous Thermal Conductivity Enhancement in Nanotube Suspensions," *Applied Physics Letters*, Vol. 79, No. 14, 2001, pp. 2252–2254.
doi:10.1063/1.1408272

[14] Das, S. K., Choi, S. U. S., and Patel, H. E., "Heat Transfer in Nanofluids—A Review," *Heat transfer engineering*, Vol. 27, No. 10, 2006, pp. 3–19.
doi:10.1080/01457630600904593

[15] Das, S. K., Choi, S. U. S., Yu, W., and Pradeep, T., *Nanofluids: Science and Technology*, Wiley, Hoboken, NJ, 2008.

[16] Eastman, J. A., Phillpot, S. R., Choi, S. U. S., Keblinski, P., Phillpot, S. R., Choi, S. U. S., and Keblinski, P., "Thermal Transport in Nanofluids," *Annual Review of Materials Research*, Vol. 34, 2004, pp. 219–246.
doi:10.1146/annurev.matsci.34.052803.090621

[17] Risha, G. A., Son, S. F., Yetter, R. A., Yang, V., and Tappan, B. C., "Combustion of Nano-Aluminum and Liquid Water," *Proceedings of the Combustion Institute*, Vol. 31, No. 2, 2007, pp. 2029–2036.
doi:10.1016/j.proci.2006.08.056

[18] Sabourin, J. L., Risha, G. A., Yetter, R. A., Son, S., and Tappan, B., "Combustion Characteristics of Nanoaluminum, Liquid Water, and Hydrogen Peroxide Mixtures," *Combustion and Flame*, Vol. 154, No. 3, 2008, pp. 587–600.
doi:10.1016/j.combustflame.2008.05.015

[19] Chon, C. H., "The Thermophysical Roll of Nanoparticles in Nanofluidic Heat and Mass Transport," Ph.D. Dissertation, Dept. of Mechanical Engineering, Univ. of Tennessee, Knoxville, TN, 2006.

[20] Lee, S., Choi, S. U. S., Li, S., and Eastman, J. A., "Measuring Thermal Conductivity of Fluids Containing Oxide Nanoparticles," *Journal of Heat Transfer*, Vol. 121, No. 2, 1999, pp. 280–289.
doi:10.1115/1.2825978

[21] Xie, H., Wang, J., Xi, T., and Liu, Y., "Thermal Conductivity of Suspensions Containing Nanosized SiC Particles," *International Journal of Thermophysics*, Vol. 23, No. 2, 2002, pp. 571–580.
doi:10.1023/A:1015121805842

[22] Murshed, S. M. S., Leong, K. C., and Yang, C., "Enhanced Thermal Conductivity of TiO_2—Water Based Nanofluids," *International Journal of Thermal Sciences*, Vol. 44, No. 4, 2005, pp. 367–373.
doi:10.1016/j.ijthermalsci.2004.12.005

[23] Gallant, R. W., "Physical Properties of Hydrocarbons. Part 37-Nitrogen Containing Compounds," *Hydrocarbon Processing*, Vol. 48, No. 8, 1969, pp. 117–126.

[24] Anon, "Physical and Thermodynamic Properties of Pure Chemicals: Data Compilation," *CH3NO2*, Taylor & Francis, Washington, D.C., 1997.

[25] Boyer, E., and Kuo, K. K., "Characteristics of Nitromethane for Propulsion Applications," 44th AIAA Aerospace Sciences Meeting and Exhibit, Reno, NV, AIAA Paper 2006-361, 2006.

[26] *CRC Handbook of Chemistry and Physics*, edited by D. R. Lide, CRC Press, Boca Raton, FL, 2007.

[27] Kim, S. J., Bang, I. C., Buongiorno, J., and Hu, L. W., "Surface Wettability Change During Pool Boiling of Nanofluids and Its Effect on Critical Heat Flux," *International Journal of Heat and Mass Transfer*, Vol. 50, No. 19–20, 2007, pp. 4105–4116.
doi:10.1016/j.ijheatmasstransfer.2007.02.002

[28] Kang, H. U., Kim, S. H., and Oh, J. M., "Estimation of Thermal Conductivity of Nanofluid Using Experimental Effective Particle Volume," *Experimental Heat Transfer*, Vol. 19, No. 3, 2006, pp. 181–191.
doi:10.1080/08916150600619281

[29] Chen, H., Ding, Y., and Tan, C., "Rheological Behaviour of Nanofluids," *New Journal of Physics*, Vol. 9, No. 10, 2007, p. 367.
doi:10.1088/1367-2630/9/10/367

[30] Hamilton, R. L., and Crosser, O. K., "Thermal Conductivity of Heterogeneous 2-Component Systems," *Industrial and Engineering Chemistry Fundamentals*, Vol. 1, No. 3, 1962, pp. 187–191.
doi:10.1021/i160003a005

[31] Das, S. K., Putra, N., Thiesen, P., and Roetzel, W., "Temperature Dependence of Thermal Conductivity Enhancement for Nanofluids," *Journal of Heat Transfer*, Vol. 125, No. 4, 2003, pp. 567–574.
doi:10.1115/1.1571080

[32] Boyer, E., and Kuo, K. K., "High-Pressure Combustion Behavior of Nitromethane," 35th AIAA/ASME/SAE/ASEE Joint Propulsion Conference, Los Angeles, AIAA Paper 99-2358, 1999.

[33] Boyer, E., and Kuo, K. K., "Modeling of Nitromethane Flame Structure and Burning Behavior," *Proceedings of the Combustion Institute*, Vol. 31, No. 2, 2007, pp. 2045–2053.
doi:10.1016/j.proci.2006.07.025

[34] Turns, S. R., *An Introduction to Combustion: Concepts and Applications*, McGraw–Hill, New York, 2000.

[35] Siegel, R., *Thermal Radiation Heat Transfer*, Taylor & Francis, London, 2002.

[36] Ichinose, N., Ozaki, Y., and Kashu, S., *Superfine Particle Technology*, Springer–Verlag, Berlin, 1992.

[37] Melius, C. F., "Thermochemistry and Reaction Mechanisms of Nitromethane Ignition," *Journal de Physique IV (France)*, Vol. 5, No. C4, May 1995, pp. C4-535–C4-552.

[38] Yamaguchi, M., "Decomposition of Adsorbed Nitromethane on γ-Alumina," *Journal of the Chemical Society, Faraday Transactions*, Vol. 93, No. 19, 1997, pp. 3581–3586.
doi:10.1039/a700059f

[39] Engelke, R., Earl, W. L., and Rohlfing, C. M., "Microscopic Evidence that the Nitromethane Aci Ion is a Rate Controlling Species in the Detonation of Liquid Nitromethane," *Journal of Chemical Physics*, Vol. 84, No. 1, 1986, pp. 142–146.
doi:10.1063/1.450189

[40] Benziger, J., "Decomposition of Nitromethane over NiO and Cr_2O_3 Catalysts," *Combustion Science and Technology*, Vol. 29, Nos. 3–6, 1982, pp. 191–205.
doi:10.1080/00102208208923597

[41] Brewster, M. Q., Hites, M. H., and Son, S. F., "Dynamic Burning Rate Measurements of Metalized Composite Propellants Using the Laser-Recoil Technique," *Combustion and Flame*, Vol. 94, Nos. 1–2, 1993, pp. 178–190.
doi:10.1016/0010-2180(93)90029-3

S. Son
Associate Editor